Journal of Materials Science and Nanotechnology
Volume 13 | Issue 1
ISSN: 2348-9812

Research Article Open Access

Keto-Enol Tautomerism and Anticancer Potential on Sudan Blue II and Synthesis and Characterisation of Sudan Blue II / Cyclodextrin doped ZnO Nanocrystals

Palanichamy Ramasamy[1], Ayyadurai Mani[1], Poomalai Senthilraja[2] and Narayanasamy Rajendiran[1,*]

[1]Department of Chemistry, Annamalai University, Annamalai Nagar, India
[2]Department of Bioinformatics, Bharathidasan University, Tiruchy, India

***Corresponding Author:** Narayanasamy Rajendiran, Department of Chemistry, Annamalai University, Annamalai Nagar, India, Tel.: +9194866 28800, E-mail: drrajendiran1967@gmail.com

Citation: Palanichamy Ramasamy, Ayyadurai Mani, Poomalai Senthilraja, Narayanasamy Rajendiran (2025) Keto-Enol Tautomerism and Anticancer Potential on Sudan Blue II and Synthesis and Characterisation of Sudan Blue II / Cyclodextrin doped ZnO Nanocrystals, J Mater Sci Nanotech nol 13(1): 101

Received Date: May 26, 2025 **Accepted Date:** July 26, 2025 **Published Date:** June 30, 2025

Abstract

Sudan blue II/cyclodextrin doped zinc oxide nanoparticles are synthesized and characterized by various spectral and microscopic methods. The doping effect of SBII/CD on ZnO nano was investigated by UV-visible, fluorescence, FTIR, DTA, XRD, FE-SEM, and TEM methods. Nanoparticle size was measured by TEM-EDS and X-RD methods. The effect of different polarities of the solvents, α-cyclodextrin (α-CD) and β-cyclodextrin (β-CD), on SBII was studied by various spectral methods. The thermodynamic properties and stability of the inclusion complexes are studied by PM3 methods. Solvent and CD studies show keto-enol tautomerism present in SBII molecules. The HOMO-LUMO gap for the SBB/β-CD inclusion complex was more negative, which supports the fact that this complex is more stable than SBB/α-CD inclusion complex. Compared to SBII/CD inclusion complex, red or blue shifted absorption and fluorescence maxima were seen in ZnO/SBII/β-CD nanoparticles. The TEM image showed that nanocrystals are formed in ZnO/SBII/β-CD. Molecular docking studies show that SBII has anticancer activity against 1r51 and 2oh4 amino acid residues.

Keywords: Sudan Blue II; Zinc Oxide nano; tautomerism; Anticancer Activity; Cyclodextrin; Nanocrystal

Introduction

Although tautomerism in phenyl azonaphthols has been recognized for over a century [1], research interest in these compounds has significantly increased only in recent decades. This growing attention is understandable: on one hand, tautomerism plays a fundamental role in biological processes and advanced technological applications [2]; on the other hand, it remains an essential area of study in the development of molecular spectroscopy techniques [3]. Notably, in many cases, individual tautomers cannot be physically separated. It is well established that tautomeric equilibrium in solution can be influenced by environmental factors such as solvent characteristics and temperature. While corresponding spectra can be recorded, they cannot always be fully analyzed using spectrophotometry alone [4].

Antonov and collaborators conducted detailed investigations into tautomeric equilibria, focusing on the quantitative effects of solvents [5] and temperature. Beyond solvent effects, the inclusion complexation of organic molecules with cyclodextrins (CDs) offers valuable insights into guest molecule geometry. CDs are water-soluble cyclic oligosaccharides known to form inclusion complexes with a wide range of organic and inorganic compounds. CDs, composed of 6–8 D-glucose units linked via α-1,4-glycosidic bonds, possess truncated cone-shaped hydrophobic cavities. These cavities can encapsulate various guest molecules in both solution and solid states, facilitating the formation of functional host–guest inclusion complexes [6], which can serve as building blocks for supramolecular assemblies.

Numerous reports of tautomers' existence can be found in the literature, although some studies fail to adequately highlight their prevalence or significance for the variations in biological activity that have been confirmed [7-12]. The significance of tautomers in the biological characteristics of prospective medications is reviewed here, along with their observation in both metalated and non-metalated substances. Based on noteworthy instances, keto-enol equilibria between imines, hydrazones, and oxindole derivatives are primarily highlighted, and methods to enhance their speciation or more clearly define their mechanisms of action are proposed.

Together with silicon dioxide and titanium dioxide nanoparticles, zinc oxide nanoparticles are thought to be among the top three most manufactured nanomaterials [13–18]. ZnO nanoparticles are most frequently used in sunscreen. They are employed because they have a large enough bandgap to be transparent to visible light while still efficiently absorbing UV light [18]. Additionally, they are being used to eradicate dangerous germs from UV-protective materials including fabrics and packaging [19-21]. It is challenging to establish claims on the production and pervasiveness of consumer items since many businesses fail to label products that contain nanoparticles [22].

Because of the reputation of the ZnO nano and SBII, this work is focused on (a) analysing whether keto-enol tautomer or intramolecular hydrogen bonding is present in SBII or not, (b) whether the spectral characteristics of SBII will be changed by the presence of CD or not, (c) whether the presence of keto and imino groups will increase or decrease the conjugation, (d) preparing ZnO nano, ZnO/CD, ZnO/SBII and ZnO/SBII/CD nanomaterials, (e) analysing the ZnO nanomaterials by various spectral and microscopic techniques and (f) evaluating the SBII antibacterial activity. Further, most of the authors analysed (g) the drug- cyclodextrin inclusion complex, which is mostly used in the medicinal and pharmaceutical fields, but, (h) in the present work, we examine how the doping of SBII/CD on ZnO modifies the nanomaterial structure. Thus, the spectral characteristics of SBII molecule have been studied in solvents of different polarity, CD and ZnO both in the S_0 and S_1 states and discussed.

Experimental

Preparation of SBII/CD inclusion complex

2×10^{-2} M concentration of SBII was dissolved in 25 mL ethanol. α-CD and β-CD (0.01 M) were dissolved in 100 mL triple dis-

tilled water. From the above α-CD and β-CD solution, pipette out different volumes (1, 2, 4, 6, 8 and 10 mL) and transfer to 10 ml standard measuring flask (SMF). To all the above 10 mL SMF, 0.2 mL of SBII solution (2×10^{-2} M) was added, then the above solutions were made up to 10 mL with triple distilled water and shaken very well. Hence, the concentration of the α-CD and β-CD solutions is 0.1×10^{-2} M to 1.0×10^{-2} M and the SBII concentration in each flask was 4×10^{-4} M. The experiments were carried out at 298 K temperature.

Preparation of ZnO and ZnO /SBII/CD nanomaterials

0.01 M of zinc sulphate was dissolved in 100 mL of deionized water and the solution was heated to 50 - 60 °C for 20 to 30 minutes. $ZnSO_4$ and NaOH solution with a molar ratio of 1:2, was carried out under vigorous stirring for 12 hrs at room temperature. The obtained white precipitate was washed several times and separated by centrifugation [23-28]. Finally, the precipitate (ZnO) was dried in an oven at 100 °C for 6 hrs. The prepared ZnO nanoparticles showed a 25-50 nm size distribution.

20 mL of 2×10^{-3} M SBII solution was added to 80 mL of 1×10^{-2} M CD solution. Then 100 mL of 0.01 M zinc sulphate (in deionized water) was added to the above SBII/CD solution. Using a hot plate with a magnetic stirrer, this mixture was heated to 50 °C for one hour. With vigorous stirring, two to five mL of 1% sodium hydroxide were added and stirred for one to two hours. After that, the above solution was frozen and dried (mini-lyophilized) at -80 °C. The powder ZnO/SBII/CD sample was collected and used for further analysis.

Molecular Modeling Studies

Theoretical calculations were carried out using the Gaussian 03W software package. The initial geometries of the SBII, α-CD and β-CD were constructed using Spartan 08 and subsequently optimized with the semiempirical PM3 method. The α-CD and β-CD structures were fully optimized using PM3 without applying any symmetry constraints. In the optimized geometry, the glycosidic oxygen atoms of the CDs were aligned on the XY plane, with their geometric center defined as the origin of the coordinate system. The primary hydroxyl groups were oriented toward the positive Z-axis.

The inclusion complexes were built using the PM3-optimized structures of the CD and the respective guest molecules. Each guest molecule was initially aligned along the Z-axis, with its longer axis placed within the CD cavity. The position of the guest was determined by selecting a specific atom and monitoring its Z-coordinate. The inclusion process was simulated by inserting the guest molecule into one end of the CD and allowing it to pass through the cavity. The PM3 method, known for its efficiency and reliability in studying the conformations of cyclodextrin inclusion complexes, was chosen to investigate the interaction of the CD with the SBII in this study.

Molecular Docking Studies

The molecular docking analysis was carried out in Dassault Systems BIOVIA Discovery Studio v22.1.100, the licensed version. Three dimensional (3D) structure of our target protein, Epidermal growth factor receptor (EGFR) complex with an epiregulin (EREG) was retrieved from Protein Data Bank (PDB) https://www.rcsb.org/(PDBID:5WB7). Protein preparation involved deleting water molecules, ions and adding hydrogen atoms. The docking was performed after grid setup was used to find optimal binding positions.

Result and Discussion

Effect of Solvents, α-CD and β-CD

The absorption and emission spectra of the sudan blue II or solvent blue 35 (1,4-bis (butyl amino) anthracene-9,10-dione (SBII,

Figure 1) were examined in different polarities of the solvents, α-CD and β-CD (Table 1, Figure 2). In all the solvents, three absorption and two emission maxima are present in SBII (cyclohexane- λabs~ 640, 594, 255 nm, and λemi~524, 338 nm; water - λabs~ 700, 630, 266 nm, λemi~430, 360, 342 nm). Interestingly, compared to other solvents, the absorption maxima were largely red shifted in water (i.e., 640 nm to 700 nm), whereas, in the excited state, the emission maxima blue shifted from 524 nm to 430 nm. Table 1 results also show that butyl substituents hardly affect the position of the keto-enol tautomeric equilibrium.

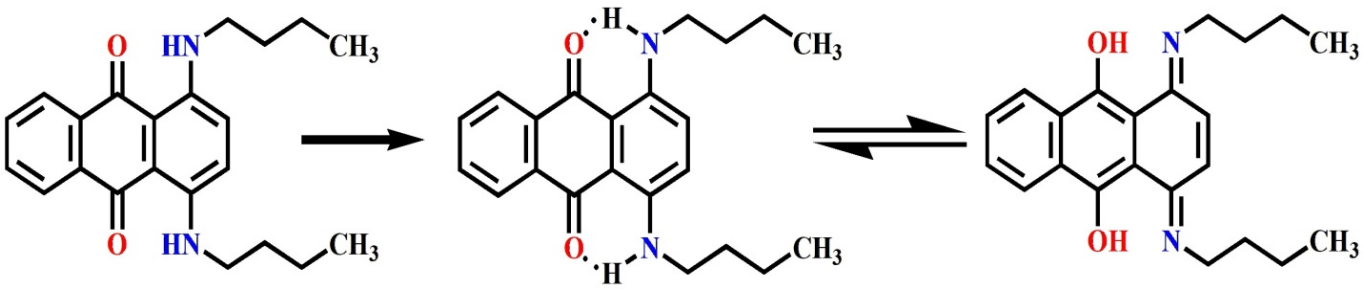

Figure 1: Keto-Enol tautomer and intramolecular hydrogen bonding structure of Sudan blue-II

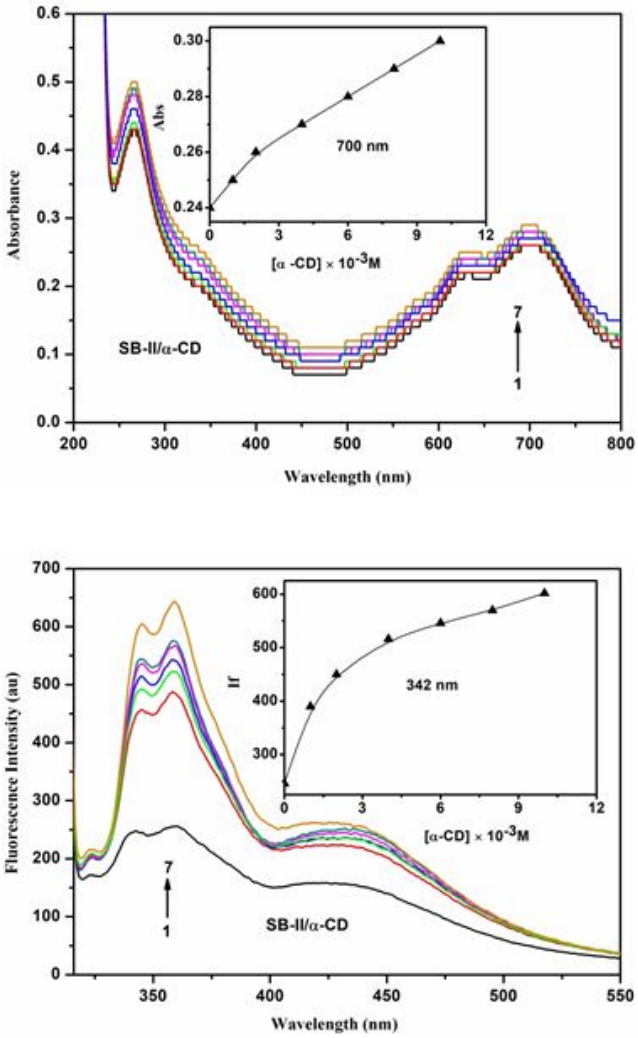

Figure 2: Absorption and fluorescence spectra of SB-II in different α-CD concentrations (M): (1) 0, (2) 0.001, (3) 0.002, (4) 0.004, (5) 0.006, (6) 0.008, (7) 0.01. Insert figure: absorbance/ fluorescence intensity vs [α-CD].

Table 1: Absorption and fluorescence spectral maxima of SB-II with different solvents, α-CD and β-CD

Solvents	λ_{abs}	log ε	λ_{flu}
Cyclohexane	640	3.3	524
	594	3.23	338
	255	3.53	
1,4-Dioxane	640	3.41	522
	594	3.34	339
	250	3.67	
Ethyl acetate	640	3.3	524
	594	3.23	427
	255	3.53	364
Acetonitrile	642	3.4	522
	595	3.34	427
	253	3.67	361
2-Propanol	644	3.34	428
	596	3.26	359
	257	3.53	
	231	2.61	
Ethanol	642	3.32	428
	595	3.23	360
	257	3.53	340
	235	3.46	
Water	700	2.79	430
	630	3.03	360
	266		342
α-CD [0.01 M]	700	2.91	430
	630	3.1	360
	266		344
β-CD [0.01 M]	700	2.87	430
	630	3.19	360
	267		342
α-CD K (1:1) x10^5 M^{-1}	52		137
β-CD K (1:1) x10^5 M^{-1}	142		174
α-CD ΔG (kcalmol^{-1})	-9		-11.4
β-CD ΔG (kcalmol^{-1})	-11.5		-12
Excitation wavelength (nm)			300

Several theories have explained this unusual red-shifted emission and absorption [29-34]. The following explanation applies to the results of our current work: (i) The large spectral shift and the broad absorption and emission spectra in SBII suggest intramolecular hydrogen bonding (IHB) or keto-enol tautomerism present in this molecule, (ii) both C=O and N-H groups form two six membered rings through IHB, and (iii) IHB formation between the C=O and N-H groups facilitates the formation of the keto-enol tautomer in the S_0 state. In other words, this hydrogen bonding makes the migration of electron density from the aromatic ring/NH group to the electron withdrawing group (C=O) more facile.

If IHB is present in SBII molecule, the absorption maxima should be blue shifted from non-polar to polar solvents because it is well known that the polar solvents affect the IHB. Increasing the polarity and proton donor capacity of the solvents, a large red shift is noticed in the absorption, but a blue shift is observed in the emission, which indicates that the keto-enol tautomer is present in the SBII molecule. Hence, the observed structured vibronic absorption and fluorescence spectral changes are interpreted as IHB associated with keto-enol tautomerism [1-12]. Increasing the polarity of solvents leads to an increase in the amount of 'keto to enol' form [1-12]. The results in Table 1 and Figure 2 predict that the C=O and NH substituents in SBII cause bathochromic shifts of the longest wavelength absorption bands for both tautomeric forms.

The results presented in Table 1 indicate that the donor substituent in SBII induces bathochromic shifts in the longest wavelength absorption bands of both tautomeric forms. A comparable trend in UV-visible spectral behavior has been observed for isomeric naphthols. Interestingly, the band positions in the UV-visible spectra show minimal dependence on solvent polarity, despite the enol tautomer being more polar and, therefore, expected to be preferentially stabilized in polar solvents. Additionally, the band maxima of individual tautomers exhibit negligible shifts across different solvents. These observations suggest that donor substituents may preferentially stabilize the enol tautomer, particularly in polar environments. Furthermore, the N···O bond distance serves as a reliable indicator of intramolecular hydrogen bond (IHB) strength, while elongation of the N–H bond due to strong hydrogen bonding is relatively minor. The data also reveal that stronger hydrogen bonding, indicated by a shorter N···O distance, is typically associated with the less stable tautomer.

In water, α-CD and β-CD, the absorption and emission maxima of SBII appear at 700, 630, 266 nm and 430, 360, 342 nm, respectively. Upon increasing the CD concentrations, no significant change was noticed in the absorption and emission wavelength, however, the emission intensity regularly increased, indicating that SBII molecules were entrapped into the CD cavities. Further, the shorter wavelength intensity increased more than that of the longer wavelength intensity. The CD cavity provides a non-polar environment and restricts the free rotation of the guest molecule; hence, the absorption and emission intensities of the SBII molecule were increased [35-46]. The absorption and emission spectral shifts and shape of SBII with α-CD or β-CD are the same, indicating that both CDs are formed by a similar type of inclusion complex. Interestingly, the structured vibronic absorption spectra noticed in the CD solutions suggest that both the keto-enol tautomer associated with the IHB is affected by the CD cavity.

Molecular Modeling

The ground state geometries of SBII, α-CD, β-CD and their inclusion complexes were optimized by the PM3 method [36-46]. HOMO, LUMO (Figure 3), energy, enthalpy, entropy, free energy, dipole moment and zero-point vibrational energy values for SBII, α-CD, β-CD and the inclusion complexes are all listed in Table 2. When SBII entered the CD cavity, the polarity and the above parameter values for SBII, α-CD, and β-CD significantly changed in the inclusion complexes. The optimization process was carried out for two sets of coordinates, beginning with the SBII molecule's aliphatic chain or anthracene ring pointing in the direction of the CD cavity. The α-CD and β-CD have interior diameters of roughly 5.6 and 6.5 Å, respectively, and heights of 7.8 Å. The vertical bond distance in SBII is 7.27 Å, and the horizontal bond length is 13.67 Å (Table 2, Figure 3). This molecule is partially enclosed in the CD cavity because the SBII horizontal bond length is greater than the size of the α-CD and β-CD cavities. The binding energy (ΔE), ΔG and ΔH values for the SBII/β-CD inclusion complexes is more negative than the

SBII/α-CD and cavity. The inclusion complexes' negative enthalpy and Gibbs energy show that the complexes form spontaneously and exothermically. The host-guest reaction (positive contribution to entropy) and the release of water molecules from the cavity (negative contribution to entropy) may work together to produce the negative entropy (ΔS) effect.

Table 2: Energetic features, thermodynamic parameters and HOMO-LUMO energy calculations for SB-II and its inclusion complexes by semiempirical PM3 method

Properties	SB-II	α-CD	β-CD	SB-II/α-CD	SB-II/β-CD
E_{HOMO} (eV)	-8.06	-10.37	-10.35	-8.27	-8.27
E_{LUMO} (eV)	-1.27	1.26	1.23	-1.40	-1.49
$E_{HOMO} - E_{LUMO}$ (eV)	6.79	-11.63	-11.58	6.86	6.78
Dipole (D)	1.86	11.34	12.29	12.19	10.80
E (kcal mol^{-1})	-47.83	-1247.62	-1457.63	-1308.94	-1511.89
ΔE (kcal mol^{-1})	-	-	-	-109.15	-102.06
G (kcal mol^{-1})	-290.76	-676.37	-789.52	-969.85	-1135.98
ΔG (kcal mol^{-1})	-	-	-	-2.72	-55.7
H (kcal mol^{-1})	-237.94	-570.84	-667.55	-829.64	-838.35
ΔH (kcal mol^{-1})	-	-	-	-20.86	-67.14
S (kcal/mol-Kelvin)	0.177	0.353	0.409	0.470	0.497
ΔS (kcal/mol-Kelvin)	-	-	-	0.06	0.089
ZPE	274.58	635.09	740.56	912.50	1140.88

kcal/mol; **kcal/mol-Kelvin; ZPE = Zero-point vibration energy

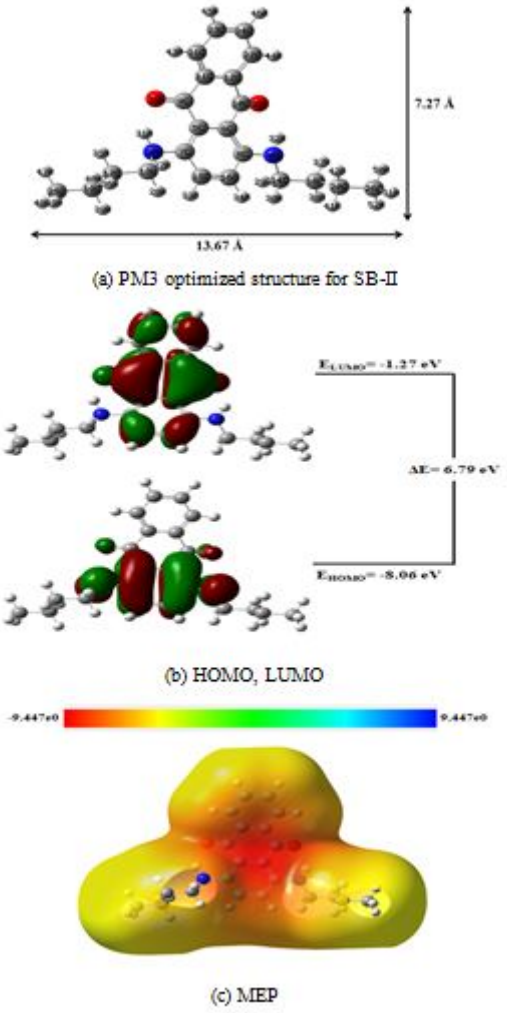

Figure 3: PM3 optimized structures of (a) SB-II, (b) HOMO, LUMO and (c) MEP of SB-II. The green and red hues in HOMO-LUMO reflect the molecules' positive and negative phases, the blue color signifies the nitrogen atom.

Figures 3 show how the HOMO-LUMO energy orbital images of each inclusion complex differ greatly from one another. The atoms' electronegative charge is higher than the other atoms, as indicated by the red hue in the molecular electrostatic potential (MEP) picture (Figure 3). Larger (EHOMO-ELUMO) values are typically more stable. The isolated SBII molecule has lower stability than the inclusion complex. The HOMO-LUMO gap for the SBII/β-CD inclusion complex was more negative, which support the fact that this complex is more stable than SBII/α-CD inclusion complexes.

Absorption and emission spectral study of ZnO nanoparticles

The absorption and emission spectra of ZnO, ZnO/SBII, ZnO/β-CD, and ZnO/SBII/β-CD nanoparticles are measured in the solution phase. ZnO nanoparticles exhibit an absorption band at 320 nm and an emission band at 420 and 355 nm, respectively. Additionally, the ZnO nanoparticles were identified by the white precipitate. It is generally accepted that the absorption and emission bands are influenced by the size, shape, metallic composition, and environment of the particles, and that the number of particles does not immediately correspond to the intensity of the absorption and emission [24-28].

When SBII was added to the ZnO nanoparticle solution, the absorption and emission maxima red shifted to 710 nm and 720, 550, 405 nm, respectively. When β-CD was doped onto the ZnO nano, the absorbance and emission maxima shifted to 250 and 398 nm, respectively. The ZnO nanoparticles' absorption maximum moved to 698 nm and their emission maxima to 655, 527,

and 415 nm, respectively, upon the addition of SBII/β-CD solution. The absorption and emission spectra's red or blue changes above imply that SBII/CD doped and interacted with the ZnO nanoparticles. In general, the intensity tends to rise or fall and the interaction is supported by spectrum fluctuations if the guest/CD cavity is doped on the nano.

3.4 FE-SEM and TEM images

ZnO nano, SBII, ZnO/β-CD and ZnO/SBII/β-CD nanomaterials were examined by FE-SEM and EDAX (Figure 4). The morphology images of the above materials demonstrate that have are different shapes. ZnO particles form small size nanoballs in a cluster shape; ZnO/β-CD is appears in a sheet shape; SBII presents in a nanorod shape; and ZnO/SBII/CD present in nanocrystal shape. FE-SEM-EDAX data predict: (a) ZnO nano contains 57.34 % zinc nano and 42.66 % oxygen, (b) ZnO/β-CD nano comprises 19.67% zinc, 54.42% oxygen and 25.91% carbon, (c) SBII dye contains 74.43 % carbon, 9.90 % nitrogen, 15.67 % oxygen, and (d) The composition of ZnO/SBII/β-CD is 12.96 % zinc, 48.54 % carbon, 4.79 % nitrogen, and 33.71 % oxygen. FE-SEM pictures and the atom composition of the nano ZnO, SBII is different from ZnO/SBII/β-CD conforms to the formation of new nanomaterials.

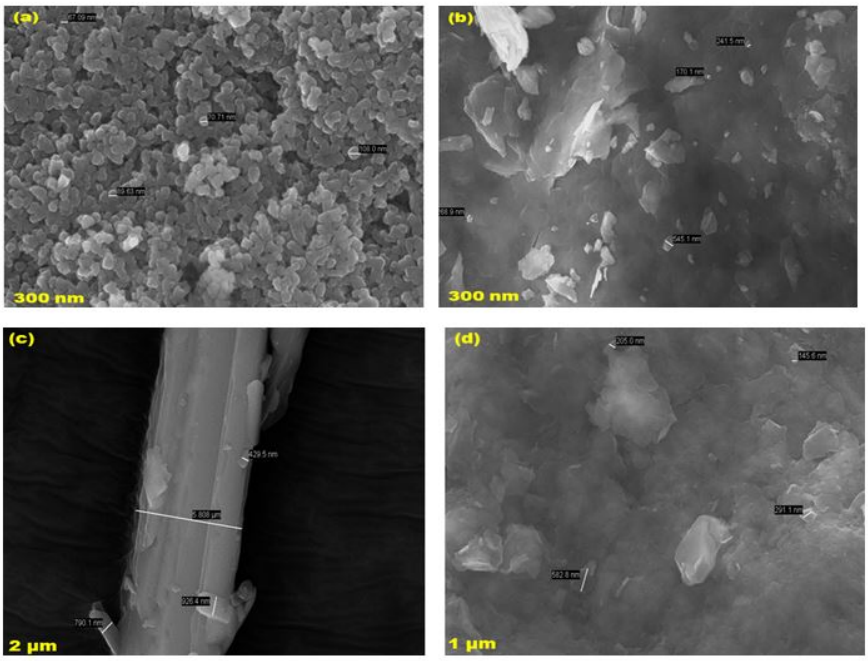

Figure 4: FE-SEM images for (a) ZnO, (b) ZnO/β-CD, (c) SB-II, (d) ZnO/SB-II/β-CD inclusion complexes.

TEM images of ZnO, ZnO/β-CD and ZnO/SBII/β-CD are displayed in Figure 5. Nanosheet like a structures are found in the ZnO nanomaterials; a nanocrystal structure is formed in ZnO/β-CD, and nano-sheet image appears in ZnO/SBII/β-CD. Uniformly spherical particles showed between 20 and 44 nm size in ZnO; 20 - 40 nm size in ZnO/β-CD and 13-24 nm size noted in ZnO/SBII/β-CD nano. The TEM-EDX data support the formation of nanoparticles: (a) ZnO nano contains 69.84 % zinc nano and 30.16 % oxygen, (b) ZnO/β-CD nano comprises 8.79 % zinc, 44.59 % oxygen and 46.61 % carbon, (c)) The composition of ZnO/SBII/β-CD is 41.57 % zinc, 9.89 % carbon, 45.46 % oxygen, and 3.08 % nitrogen. The presence of ZnO along with SBI-I/β-CD is confirmed by the EDX data for the nanocrystals.

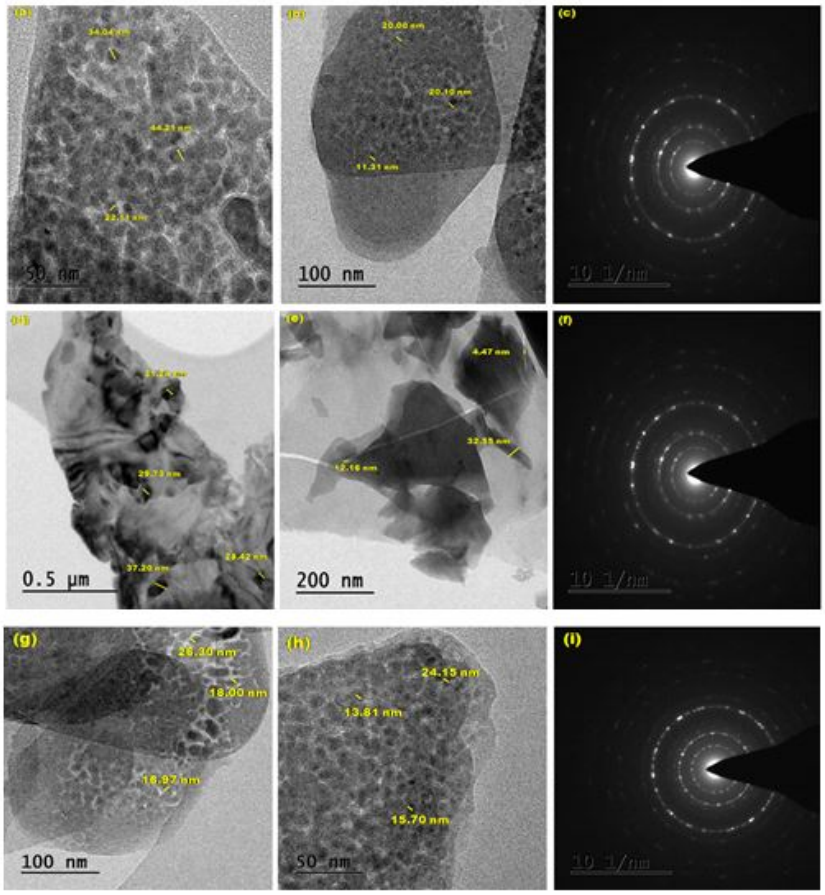

Figure 5: HR-TEM images for (a-c) ZnO, (d-f) ZnO/β-CD, (g-i) ZnO/SB-II/β-CD

Powder X-Ray Diffractogram

The standard ZnO face-centered cube peaks of the JCPDS card 800-075 were used to index all the diffraction peaks. The formation of the hexagonal tightly packed (HCP) structure and the mineral designation (3C) have been verified using the JCPDS: 03-065-3411 data. The XRD pattern of ZnO nanoparticles is produced at 60° and the hkl plane values were located at the hexagonal structure of ZnO's (100), (002), (101), (102), (103), (110), (112), and (201) reflection planes. In ZnO, eight diffraction peaks located at 31.80, 34.51, 36.21, 47.52, 56.61, 62.90, 67.91, 69.92 and in β-CD, eight peaks were observed at 13.39, 19.93, 23.50, 27.65, 31.96, 35.54, 40.58, 48.90 while in ZnO/β-CD ten peaks formed at 10.15, 15.18, 25.41, 28.38, 34.92, 42.29, 49.77, 59.16, 63.32, 70.33. In SBII, nine peaks were formed at 7.90, 12.61, 17.45, 19.88, 22.90, 25.60, 28.80, 36.45, 48.19 and in ZnO/SBI-I/β-CD eleven peaks formed at 10.60, 15.85, 25.82, 29.05, 33.60, 35.11, 36.86, 42.65, 50.20, 59.11, 63.35. The diffraction pattern and the peak intensities of ZnO/SBII/β-CD nanomaterials differed from those of isolated SBII, indicating the formation of nanomaterials. Additionally, several conspicuous peaks that enable the production of ZnO/SBII/β-CD nanocrystals emerge in the 10–80 degree range.

The nanoparticle size is also measured in X-RD and HR-TEM methods. In XRD, the Scherer equation is used [$D = K\lambda/\beta Cos\theta$]. D = average particle size, K = constant value (0.94). The particle sizes are given below: ZnO nano – 19.30 nm, β-CD – 23.84, SBII- 25.62 nm, ZnO/β-CD - 20.69 nm, and ZnO/SBII/β-CD Nano – 18.10 nm. In HR-TEM, the particle sizes are measured by IMAGE-J software and the average particle size is calculated by Origin software. The particle size is given below: ZnO nano – 24.98 nm, ZnO/β-CD – 23.98 nm, ZnO/SBII/β-CD Nano – 19.18 nm. Compared to XRD method, 1-2 nm particle size is varied in the HR-TEM method.

Infrared Spectral Studies

FTIR spectra of ZnO nano, SBII, ZnO/SBII, ZnO/β-CD and ZnO/SBII/β-CD were measured. Due to the conversion of Zn^{+2} to ZnO nanoparticles, the FTIR frequencies of the ZnO nanoparticles were observed at 3325, 1587, 1450, 592, and 513 cm^{-1}. The frequencies that appear at 3325 cm^{-1} indicate the presence of ZnO and the peaks at 592, and 513 cm^{-1} suggest the presence of Zn nanoparticles. It has already been reported that the FTIR peak of pure ZnO nanoparticles that appears at 595 cm^{-1} was the characteristic absorption of the ZnO bond and the broad band peak at 3507 cm^{-1} can be attributed to the characteristic absorption of O-H group.

When zinc oxide nano added to β-CD, 3325 cm^{-1} frequency shifts to 3280 cm^{-1}, while 1587, 1450 cm^{-1} move to 1614, 1514 cm^{-1} and 592, 513 cm^{-1} peaks shift to 594, 526 cm^{-1}. The above variation in the FTIR frequencies indicates that ZnO nanoparticles are doped by the CD. In SBII, the NH group stretching frequency appears at 3275 cm^{-1}, CH_2 and CH_3 deformation frequencies appear at 1454 and 1360 cm^{-1}, respectively, and the C=O stretching frequency appears at 1650 cm^{-1}. Aromatic ring stretching frequency appears at 1628 cm^{-1}. The C-N frequency appears at 1134 cm^{-1}, out of plane C-H bending frequencies appear at 894, 804 cm^{-1} and C-N-C bending frequency appears at 547 cm^{-1}.

When SBII/β-CD added to ZnO nano particles, the above frequencies are shifted to lower or higher wave numbers. In ZnO/SBII/CD, the NH group stretching frequency moves to 3282 cm^{-1}, CH_2 and CH_3 deformation frequencies appear at 1458 and 1360 cm^{-1}, respectively and C=O stretching frequency appears at 1643 cm^{-1}. Aromatic ring stretching frequency appears at 1614 cm^{-1}. C-N frequency appears at 1118 cm^{-1}, out of plane C-H bending frequency appears at 956 cm^{-1} and C-N-C bending frequency appears at 594 cm^{-1}. Compared to SBII and ZnO/β-CD, ZnO/SBII/β-CD nanocrystals showed a marked change in the frequencies, suggesting that the ZnO nanoparticles interact with the SBII and β-CD.

DTA Thermogram

DTA profiles of pure ZnO nano, SBII, ZnO/β-CD and ZnO/SBII/β-CD are analysed. In ZnO nano, two exothermic and three endothermic peaks were noticed at 226.1, 546.7 °C and 272.6, 731.1, 919.2 °C, respectively. SBII exhibits two exothermic and one endothermic peaks at 565.8, 800.2 °C and 680.4 °C, respectively. β-CD exhibits one exothermic peak at 128.6 °C. The results suggest water molecules are not present in β-CD. In ZnO/β-CD, two exothermic and four endothermic peaks appear at 224.3, 932.4 °C and 265.2, 354.6, 749.8, 884.1 °C, respectively. In ZnO/SBII/β-CD, three endothermic and four exothermic peaks appear at 270.3, 385.1, 945.4 °C, and 209.7, 327.3, 725.7, 985.7 °C, respectively. The endothermic peaks in the nanomaterials are caused by the loss of water from the CDs. In contrast to the pure SBII and ZnO, a new peak arises in ZnO/SBII/β-CD confirming the formation of the nanocrystals. Because of doping, the various spectral (UV-visible, fluorescence, FTIR, DTA, PXRD), and microscopic images (SEM, TEM) of ZnO/SBII/β-CD vary from SBII, β-CD to ZnO.

Anticancer Activity by Molecular Docking

Molecular docking of SBII was given in Figures 6 and 7. In the figure, A and B show the 3D and 2D interactions of the Epidermal growth factor receptor (EGFR) complex with epiregulin (EREG) (PDB ID:5WB7) with SBII. The amino acid interactions of target proteins with SBII are given below (ID No. 3766139): SBII with 1r51 amino acid residues - two π – π stacked interactions noticed at Phe159, while π-alkyl interactions observed at Arg176, Leu 170, Val227 & Ile228 and the LibDock score is 86.31. Further, SBII with 2oh4 amino acid residues – a carbon-hydrogen bond is noticed at Cys1043 while π-alkyl interaction is observed at Leu887, Ile886, Leu1017 & Cys1022 and the LibDock score is 101.63.

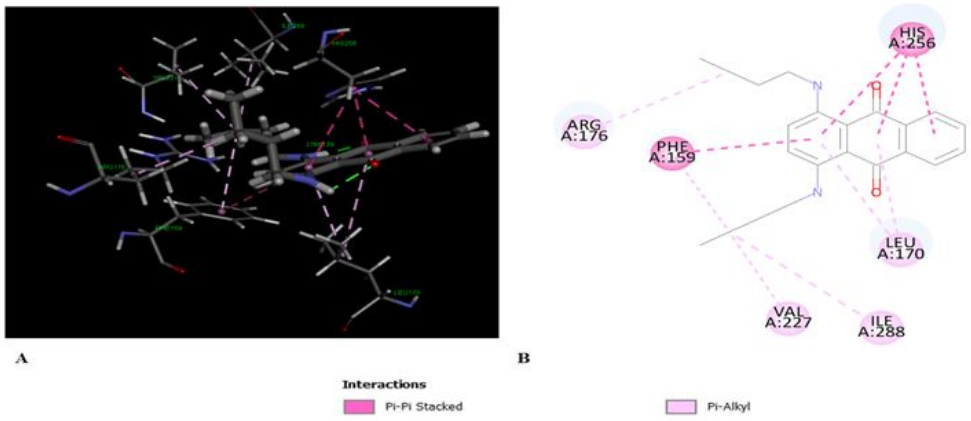

Figure 6: Anticancer activity of SBII by molecular Docking method (SBII interacting with 1r51 amino acid residues)

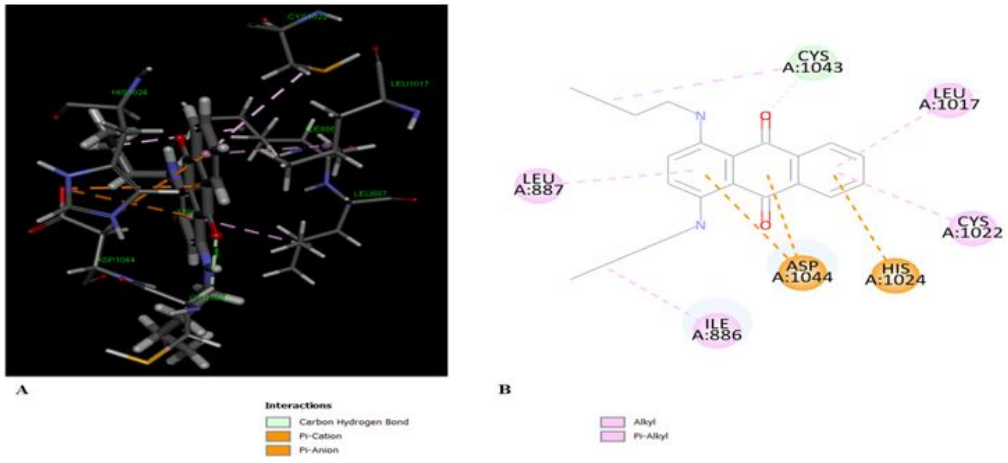

Figure 7: Anticancer activity of SBII by molecular Docking method (SBII interacting with 2oh4 amino acid residues)

From the auto dock method, the following anticancer test values are noticed for SBII: ADMET solubility level is 2 (Absorption–Distribution–Metabolism–Excretion–Toxicity are the internal processes that describe how a drug moves throughout and is processed by the body), ADMET BBB level is 1 (Blood Brain Barrier is a term used to describe the particular properties of the central nervous system (CNS) vasculature), ADMET EXT Hepatotoxic applicability# MD is 9.15047 respectively. Drug-induced hepatotoxicity is an acute or chronic liver injury secondary to drugs or herbal compounds. It is difficult to diagnose. Further, ADMET EXT CYP2D6# Prediction is true, ADMET EXT Hepatotoxic# Prediction is true and ADMET EXT PPB# Prediction is true. siRNA Plasma Protein Binding (PPB) is a measure of the unbound fraction (fu) of siRNA in plasma at equilibrium. A PPB report is required for small molecule regulatory filing because, according to the free drug hypothesis, fu plasma is equivalent to the unbound drug concentration at the site of action in a steady state. The above results show that SBII has anticancer activity.

Conclusion

ZnO/Sudan Blue II/CD nanoparticles are synthesized and characterized by spectral and microscopic methods. Solvent and CD studies show keto-enol tautomerism is present in SBII molecules. The structured vibronic absorption spectra noticed in the CD solutions suggest that both the keto-enol tautomer associated with the IHB is affected by the CD cavity. The PM3 method shows that the SBII molecule is partially encapsulated in the CD cavity. The HOMO-LUMO values indicate that the SBII/β-CD

inclusion complex is more stable than SBII/α-CD. Red or blue shifted absorption and fluorescence maxima were seen in ZnO/SBII/β-CD rather than SBII/CD, suggesting that nanocrystals are formed. Nanoparticle size was measured by TEM-EDS and X-RD methods. TEM images showed that nanocrystals are formed in ZnO/SBII/β-CD. Molecular docking studies show SBII has anticancer activity against 1r51 and 2oh4 amino acid residues.

Acknowledgement

This work was supported by the Rashtriya Uchchatar Shiksha Abhiyan (RUSA) Phase -2.0 [No. 128/A1/ RUSA 2.0, Health and Environment] New Delhi, India

Declaration of Competing Interest

The authors declare no conflict of interest

Data Availability

No data was used for the research described in the article

References

1. Zollinger H (2009) Colour chemistry, synthesis, properties and applications of organic dyes and pigments, (3ed) verlag Helvetica Chimica Acta., Zurich, 429.

2. Antonov L, Fabian FMW, Taylor JP (2005) Tautomerism in some aromatic Schiff bases and related azo compounds: an LSER study. J Phys Org Chem, 18:1169.

3. Antonov L, Kawauchi S, Satoh M, Komiyama J (1999) Ab initio modeling of the solvent influence on the azo–hydrazone tautomerism, Dyes and Pig, 40:63.

4. Antonov L, Nedeltcheva D (2009) Resolution of overlapping UV–Vis absorption bands and quantitative analysis. Chem Soc Rev, 29: 217.

5. Szejtli J, Osa T (1996) In Comprehensive Supramolecular Chemistry ed. Atwood JL, Davies JE, MacNicol DD, Vogtle F Pergamon/Elsevier, Oxford, 3.

6. Ivanova D, Deneva V, Nedeltcheva D, Kamounah FS, Gergov G et al. (2015) Tautomeric transformations of piroxicam in solution a combined experimental and theoretical study. RSC Adv, 5: 31852-860.

7. Deneva V, Slavova S, Kumanova A, Vassilev N, Nedeltcheva-Antonova D et al. (2022) Favipiravir—Tautomeric and Complexation Properties in Solution. Pharmaceuticals, 16: 45-57.

8. Dhaked DK, Guasch L, Nicklaus MC (2020) Tautomer Database: A Comprehensive Resource for Tautomerism Analyses. J. Chem. Inf. Model, 60: 1090-100.

9. Katritzky AR, Hall CD, El-Gendy BEDM, Draghici B (2010) Tautomerism in drug discovery J.Comput. AidedMol.Des, 24: 475-84.

10. Wang X, Zhao W, Al-Abdul-Wahid S, Lu Y, Cheng T, Madsen J (2021) Trifluorinated Keto–Enol Tautomeric Switch in Probing Domain Rotation of a G Protein-Coupled Receptor, J Bioconjugate Chem, 32: 99-105.

11. Ana Paula Araujo de Oliveira, Camila Anchau Wegermann, Ana Maria Da Costa Ferreira (2024) Keto-enol tautomerism in the development of new drugs Front. Chem. Biol, 3: 1-7.

12. Surabhi Siva Kumar, Putcha Venkateswarlu Rao, Vanka Ranga Rao, Nageswara Gollapalli (2013) Synthesis, characterization and optical properties of zinc oxide nanoparticles International Nano Letters, 3: 30-35.

13. Yuanyuan Zhang, Yu-Rui Leu, Robert Aitken J, Michael Riediker (2015) Inventory of Engineered Nanoparticle-Containing Consumer Products Available in the Singapore Retail Market and Likelihood of Release into the Aquatic Environment International J Environmental Research and Public Health, 12: 8717-743.

14. Fabiano Piccinno, Fadri Gottschalk, Stefan Seeger, Bernd Nowack (2012) Industrial production quantities and uses of ten engineered nanomaterials in Europe and the world J Nanoparticle Research, 14: 1109-15.

15. Sukesh Kashiram Tumram, Rajdip Bandyopadhyaya (2023) Zinc oxide nanostructures: Experiments probing their transformation to nanorods, Materials Science and Engineering: B, 296: 116569.

16. Arturo Keller A, Suzanne McFerran, Anastasiya Lazareva, Sangwon Suh (2013) Global life cycle releases of engineered nanomaterials J Nanoparticle Research, 15: 1692-4.

17. Rebecca Kessler (2013) Engineered Nanoparticles in Consumer Products: Understanding a New Ingredient Environmental Health Perspectives, 119: A120-125.

18. Cristina Iosub Ş. Elena Olăreţ, Alexandru Mihai Grumezescu, Alina Holban M, Ecaterina Andronescu (2017) Chapter 29 - Toxicity of nanostructures—a general approach. Nanostructures for Novel Therapy, Nanostructures for Novel Therapy, Synthesis, Characterization and Applications, Micro and Nano Technologies Elsevier, 793-809.

19. Noorian SA, Hemmatinejad N, Navarro JAR (2020) Ligand modified cellulose fabrics as support of zinc oxide nanoparticles for UV protection and antimicrobial activities International J biological macromolecules, 154: 1215-226.

20. Seyyed Abbas Noorian, Nahid Hemmatinejad (2015) Azadeh Bashari One-Pot Synthesis of Cu2O/ZnO Nanoparticles at Present of Folic Acid to Improve UV-Protective Effect of Cotton Fabrics Photochemistry and Photobiology, 91: 510-7.

21. Matthew Hull S, David Rejeski Jr F, Michael Hochella F, Sean McGinnis P, Eric Vejerano P, Todd Kuiken (2015) Nanotechnology in the real world: Redeveloping the nanomaterial consumer products inventory Beilstein J Nanotechnology, 6: 1769-780.

22. Surabhi Siva Kumar, Putcha Venkateswarlu, Vanka Ranga Rao, Gollapalli Nageswara Rao (2013) Synthesis, characterization and optical properties of zinc oxide nanoparticles. International Nano Letters, 3: 30-5.

23. Ramasamy P, Mani A, Sneha B, Nivetha E, Venkatesan M, Rajendiran N (2025) Azo-hydrazo tautomerism in Sudan Red-B and Cyclodextrin/ Sudan Red-B doped ZnO nanomaterials, J Molecular Structure, 1329: 141423- 431.

24. Mani A, Ramasamy P, Antony Muthu Prabhu A, Rajendiran N (2023) Investigation of Ag and Ag/Co bimetallic nanoparticles with naproxen-cyclodextrin inclusion complex. J Molecular Structure, 1284: 135301-10.

25. Mani A, Venkatesh G, Senthilraja P, Rajendiran N (2024) Synthesis and Characterisation of Ag-Co-Venlafaxine-Cyclodextrin Nanorods. European J Advanced Chemistry Research, 5: 9-16.

26. Mani A, Ramasamy P, Antony Muthu Prabhu A, Senthilraja P, Rajendiran N (2024) Synthesis and Analysis of Ag/Olanzapine /Cyclodextrin and Ag/Co/Olanzapine /Cyclodextrin Inclusion Complex Nanorods. Physics and Chem. Liquids, 62: 196-209.

27. Mani A, Ramasamy P, Antony Muthu Prabhu A, Senthilraja P, Rajendiran N (2005) Synthesis and Characterisation of Ag/-Co/Chloroquine/Cyclodextrin Inclusion Complex Nanomaterials J Sol-Gel Science and Technology.

28. Lippert E, Lunder W, Boos H (1962) In: Mangini A (Ed.) Advances in Molecular Spectroscopy, Pergamon Press, Oxford, p. 1962; 443. doi.org/10.4236/ojpc.2012.24029

29. Khalil OS, Meeks JS, McGlynn SP (1976) Electronic states and "Geometric Isomerism" of p-disubstituted cyanoanilines Chem. Phys. Lett, 39: 457-61.

30. Kosower EM, Dodiuk H (1976) Multiple fluorescence. II. A new scheme for 4-(N,N-dimethyl amino)benzonitrile including proton transfer J. Am. Chem. Soc, 98: 924-9.

31. Chandros A (1975) In: Gordon M, Ware M (Eds.), Exciplex, Academic Press, New York, 187.

32. Visser RJ, Wiesenborn PCM, Varma CAGO (1985) Solute-solvent exciplexes as the source of anomalous fluorescence from 4-N,N-dimethylamino-ethylbenzoate in 1,4-dioxane and in polar solvents. Chem. Phys. Lett, 113: 330-6.

33. Rettig W (1986) Charge Separation in Excited States of Decoupled Systems—TICT Compounds and Implications Regarding the Development of New Laser Dyes and the Primary Process of Vision and Photosynthesis Angew. Chem. Int. Ed. Engl, 25: 981-8.

34. Antony Muthu Prabhu ., Venkatesh G, Sankaranarayanan RK, Rajendiran N (2010) Azonium-ammonium tautomerism and inclusion complexation of 4-amino-2', 3-dimethyl azobenzene Indian J. Chem, 49A: 407-17.

35. Antony Muthu Prabhu A, Venkatesh G, Rajendiran N (2010) Azo-Hydrazo tautomerism in 1-phenyazo-2-naphthol dyes in various solvents, pH and β-CD. J. Fluorescence, 20: 961-72.

36. Venkatesh G, Antony Muthu Prabhu A, Rajendiran N (2011) Azonium-Ammonium Tautomerism and Inclusion Complexation of 1-(2,4-diamino phenylazo) naphthalene and 4-Amino azobenzene. J. Fluorescence, 21: 1485-497.

37. Prema Kumari J, Antony Muthu Prabhu A, Venkatesh G, Subramanian VK, Rajendiran N (2011) Effect of solvents and pH on β-CD Inclusion complexation of 2,4-dihydroxy azobenzene and 4-hydroxy azobenzene. J. Solution Chem, 40: 327.

38. Rajendiran N, Sankaranarayanan RK, Venkatesh G (2014) Cyclodextrin covered organic micro rod and micro sheet derived from supramolecular self assembly of 2,4-dihydroxy azobenzene and 4-hydroxy azobenzene inclusion complexes Bull Chem Soc Japan, 87: 283-93.

39. Rajendiran N, Sankaranarayanan RK (2014) Azo dye/Cyclodextrin: New findings of identical nanorods through 2:2 inclusion complexes Carbohydrate Polymers, 106: 422-31.

40. Rajendiran N, Sankaranarayanan RK (2015) Nanorod formation of cyclodextrin covered sudan dyes through supramolecu-

lar self assembly J. Experimental Nanoscience, 10: 407-28.

41. Rajendiran N, Sankaranarayanan RK, Saravanan J (2015) Nanochain and vesicles formed by inclusion complexation of 4, 4'-diamino benzanilide with Cyclodextrins. J. Experimental Nanoscience, 10: 880-99.

42. Venkatesh G, Thulasidhasan, J, Rajendiran NA (2022) Spectroscopic and molecular modeling studies of the inclusion complexes of orciprenaline and terbutaline drugs with native and modified cyclodextrins. J. Inclusion Phenomena and Macrocyclic Chemistry, 78: 225-37.

43. Rajendiran N, Venkatesh G (2014) Inclusion complexation of 4,4'-dihydroxy benzophenone and 4-hydroxy benzophenone with α- and β-CD. Supramolecular Chemistry, 26: 783-95.

44. Rajendiran N, Sankaranarayanan RK, Saravanan J (2014) Nanostructures formed by cyclodextrin covered amino benzophenones through supramolecular self assembly, Spectrochim Acta A, 127: 52-60.

45. Jude Jenita M, Mohandoss T, Rajendiran N (2014) Spectral and molecular modeling studies on hydroxy benzaldehydes with native and modified cyclodextrins, J. Fluorescence, 24: 695-707.